

Self-healing polymers: evaluation of self-healing process via non-destructive techniques

D. G. Bekas¹, D. Baltzis¹, K. Tsirka¹, D. Exarchos¹, T. Matikas¹, A. Meristoudi², S. Pispas² and A. S. Paipetis^{*1} 

The scope of this study is the real-time monitoring and evaluation of the healing process using novel testing procedures and non-destructive evaluation techniques. In this work, the healing approach that has been followed is that of the intrinsic Diels–Alder (DA) and retro-DA mechanism. Two polymers were used as adhesives in single lap-joint specimens that were subjected to static tensile loading. The healed specimens were subjected to the same testing procedure as the one before the first failure and the healing efficiency was assessed by the correlation of the experimental results prior and after healing. Acoustic emission and infrared thermography were employed with the destructive tests so as to monitor changes in the acoustic and the thermal profile between the virgin and the ‘healed’ specimen.

Keywords: Self-healing polymers, Diels–Alder mechanism, Non-destructive evaluation

Introduction

One of the most outstanding features of biological organisms is their ability to self-repair damage, such as cuts or bruises which are often healed with full restoration. The effort to impart similar properties to man-made materials and particularly to polymers led the research community towards the design of multifunctional polymers that are capable of regaining their initial properties after damage. The self-healing functionality may be achieved via thermally reversible reactions. These reactions include the Diels–Alder (DA) reaction for cross-linking linear polymers. The DA reaction has been extensively studied by many research groups as theoretically it may provide infinite number of repetitions of the healing process without any further addition of chemicals or healing agents.^{1–10}

Toncelli *et al.*¹¹ presented the successful synthesis and cross-linking of functionalised (varying amounts of furan groups) polyketones with (methylene-di-*p*-phenylene)bis-maleimide. In addition, they managed to modify thermal and mechanical properties of the material by controlling the furan reactions. This self-healing polymer exhibited an almost full recovery of thermal and mechanical properties for seven consecutive self-healing cycles, independently of the furan intake. In another study, Rivero *et al.*¹² managed to produce polyurethane networks with healing capability at mild temperature conditions. A combination of a quick shape memory effect (contact

of the free furan and maleimide moieties) followed by a progressive DA reaction (reformation of the covalent bonds) allowed the re-mendable process to take place in temperatures as low as 50°C, achieving a full recovery of the structural properties without complete melting of the polymer.

Adhesive shear strength is of vital importance when self-healing materials are used as adhesives in lap joints of various adherents. Due to its simplicity, the single lap-joint shear testing is a very popular test to assess adhesion efficiency. It is well known that various parameters such as adherent material and surface morphology^{13,14} of the employed self-healing adhesive¹⁵ can seriously affect the adhesive strength. For instance, Aubert¹⁶ employed the lap-shear test in order to assess the healing performance of self-repairing adhesives based on the DA reaction. In this study, aluminium and steel adherents were used and a commercially available elastomeric adhesive was used for comparison reasons. Both the elastomeric- and the DA-based adhesives exhibited similar average shear strengths when used with aluminium and steel adherents but the DA adhesive exhibited lower deviation for the two different adherents.

It is well known that the initiation and propagation of cracks within a material under stress invokes stress waves that propagate within the material known as acoustic emission (AE). Moreover, it is well established by now that the features of the propagated transient waveform of the material depend on the type of failure providing to it, if not a unique, a distinct acoustic signature. To this end, AE has been employed in order to monitor the fracture process of structural materials and build an understanding on the damage behaviour of materials under stress.^{17,18} The potential of AE for monitoring the healing

¹Department of Material Science and Engineering, University of Ioannina, Ioannina 45110, Greece

²Theoretical and Physical Chemistry Institute, National Hellenic Research Foundation, 48 Vassileos Constantinou Avenue, Athens 11635, Greece

*Corresponding author, email paipetis@cc.uoi.gr

process lies within the identification of the features that alter the acoustic signature of the material in successive healing cycles. The acoustic signature is expected to change because the healing functionality of the material is well known to decrease with successive healing cycles and is not in reality a reversible process. This gradual healing functionality loss is expected to affect distinct descriptors of the transient AE waveform like the central frequency, the absolute energy, the hits activity, etc.

In addition to AE, qualitative evaluation of the self-healing efficiency can also be accomplished via infrared thermography (IRT). Combined IRT and AE has been successfully employed to monitor the efficiency of bonded repairs of carbon fibre reinforced panels.¹⁹ IRT has been extensively employed to monitor damage mostly manifested as a local differentiation in the thermal diffusivity properties of damage sites within the material. Maldague²⁰ showed that pulsed thermography is a quick and reliable tool to identify defects in various materials such as metals, ceramics and polymers. Several IR thermographic techniques have been employed in order to identify subsurface defects²¹ in composite materials either off-line or on-line.²² Chowdhury *et al.*²³ have successfully evaluated the self-healing efficiency of fibre reinforced composites via the employment of optical IRT. In their study, glass fibre reinforced composites containing 30% of urea-formaldehyde microcapsules were subjected to low velocity impact and subsequent healing recovery observed in terms of damaged area reduction.

Summarising, the scope of the current study is to effectively monitor the self-healing process of self-healing adhesives based on the DA reaction. To this end the single lap-joint shear test was employed, where the adhesive was a commercial BMI system with a trifuran (TF) compound employed as a cross-linker. Both AE and IRT were employed to evaluate the healing process. The acoustic activity of the lap-shear coupon was recorded during loading for successive healing cycles. In a parallel study, the self-healing polymer was monitored via IRT in order to assess the induced changes after a healing event.

Experimental

Materials

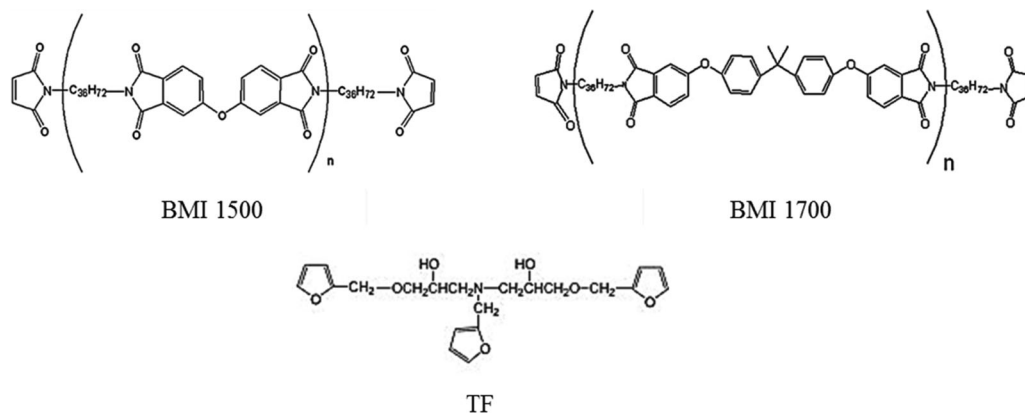
The materials used in the current study are two bis-maleimide terminated polyimide resins, BMI-1500 and BMI-

1700, supplied by Designer Molecules Inc., USA. With molecular weights approximately 1500 and 1700 Da, respectively, as denoted by their names, their main difference lies in their viscosity. As for their main characteristics, these include superior thermal stability and high adhesion to various substrates.

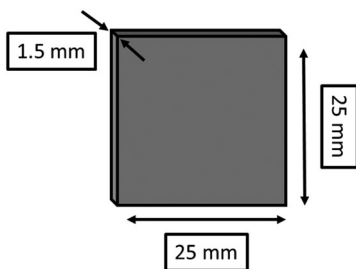
A TF compound was selected as the cross-linker in both systems. The cross-linker preparation was done according to the procedure proposed by Liu and Hsieh.²⁴ In more detail, furfuryl glycidylether (20 mmol) and furfuryl amine (10 mmol) were dissolved in 25 mL toluene and left to react at 110°C for 3 h in dark. Then, the solvent was evaporated and the product was washed with 30 mL of *n*-hexane for three times and dried under vacuum at ambient conditions for 36 h. The product was a viscous liquid. Figure 1 depicts the molecular structure of the two oligomers and the TF compound.

The mixing ratio of the aforementioned components was 5.71:1 for TF/BMI-1500 and 6.53:1 for TF/BMI-1700 by weight. Subsequently, the mixed components were used as an adhesive in a metal-to-metal lap-shear geometry according to ASTM D 1002.²⁵

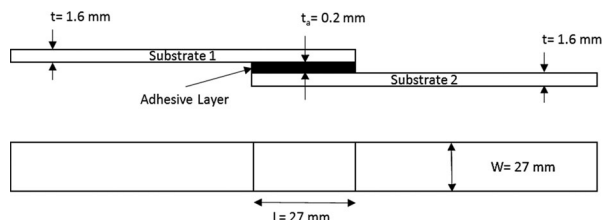
Anodised Al 2024 T3 has been used as the substrate for this study. Anodising and surface preparation was performed in house according to ASTM D3933.²⁶ The procedure included roughening of the substrate surface using 180-grit sand paper for 5 min and then cleaning by immersion first in distilled water and then in acetone. Subsequently, the anodised plates were immersed in a sodium hydroxide solution (5 wt-% NaOH) for 10 min at room temperature and afterwards in distilled water for 5 min at 43°C. Deoxidation was performed by immersion in a nitric acid solution (50 wt-% HNO₃) for 10 min at ambient conditions followed by cleaning with distilled water for 5 min at 43°C. Anodising was carried out in a phosphoric acid solution (10 wt-% H₃PO₄) for 20 min at ambient conditions followed by immersion in distilled water for 10 min at 43°C. Single rack configuration was used, with applied voltage of 10 V for 20 min. Finally, the specimens were dried in clean air for 30 min at 80°C and afterwards the commercial BR127 epoxy primer coating by CYTEC was applied on the anodised layer using a spray gun, in order to seal the anodised layer and ensure maximum adhesion between the adhesive and the adherent. The specimen's geometry is depicted in Fig. 2 where the substrate material is the primer-coated aluminium and the adhesive layer consisted of the two studied polymers.



1 The molecular structure of the re-mendable oligomers BMI-1500 and BMI-1700 and the TF compound



2 Film's dimensions



3 Lap-shear geometry

For the manufacturing of the film that has been tested via off-line IRT, BMI-1700/TF mixture was casted in a silicon rubber mould (Rhodorsil RTV 3325/Rhodorsil cata 24 h) and heated up to 160°C for 6 h using a laboratory oven. At the end of the heating process the produced polymeric film was left to cool down for several hours at room temperature. A small artificial defect of approximately 2 mm length was created with a scalpel on the surface of the specimen in order to monitor the response of the defect area after a single healing process. Figure 2 depicts the dimensions of the produced film.

For the manufacturing of the single lap-joint specimens, the two oligomers were heated up to 100°C separately in order to reduce their viscosity. The appropriate amount of TF was added to the BMIs and mixed until two homogenised mixtures were produced (BMI-1700/TF and BMI-1500/TF). The produced mixtures were then instantly spread on the single lap bond area and the specimens assembly was heated to 160°C using a hot press for 6 h. Spacers were used in order to maintain the adhesive thickness at 200 μm . Specimens were left to cool down at ambient temperature for the appropriate

amount of time. A total amount of five specimens for each polymeric system were manufactured. Figure 3 depicts the lap-shear geometry that have been used in the mechanical testing.

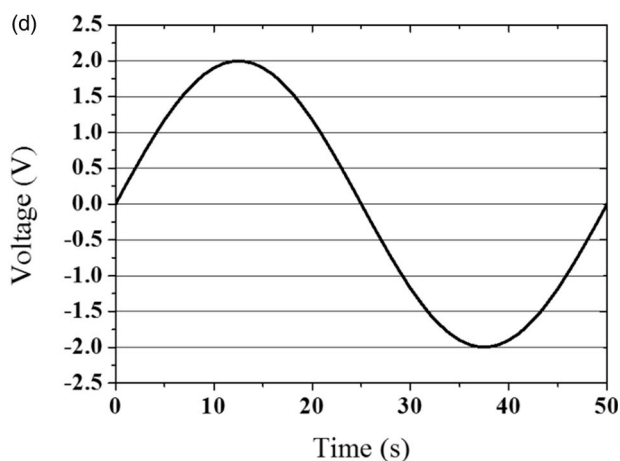
IRT

For the acquisition of the thermal dynamic response, the Jade 510-CEDIP-MIR infrared camera was employed, as shown in Fig. 4. It employs a cooled indium antimonide detector (3–5 μm), with a frame rate ranging from 50 to 150 Hz and focal plane array pixel format of 320 (H) \times 240 (V). The camera was employed to assess the healing efficiency of one of the polymers, BMI-1700. More specifically, employing the pulse thermography method. IR lamps were used as heating source, and the excitation was a single period of a sinusoidal wave of 0.02 Hz (duration 50 s) and the peak-to-peak voltage was 2 V (Fig. 4d). The sinusoidal excitation was used, as periodical heating was experimentally found to result in a more uniformly heated specimen.

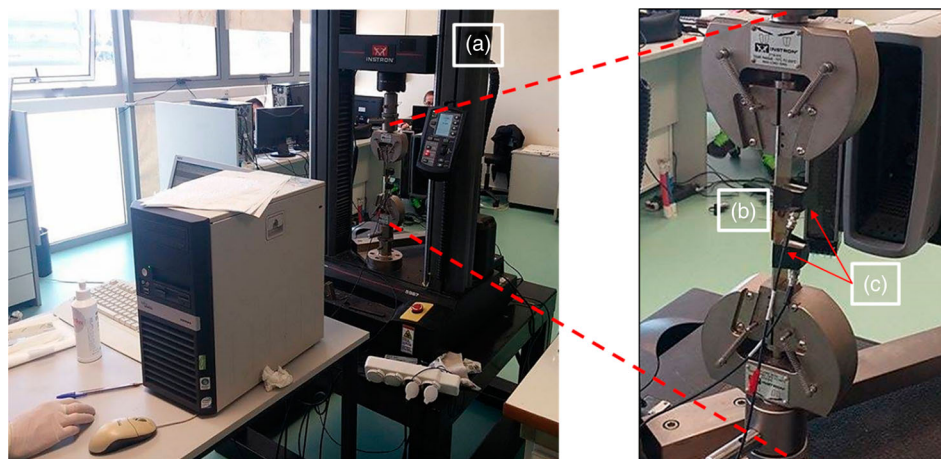
The distance between the material and the lamps as well as the IR camera was 40 cm. In addition, the recording duration of the IR camera was 150 s in order to monitor an entire period of heating and cooling. Post-processing in order to obtain phase/amplitude images consisted in the Fast Fourier Transform of the acquired thermographs at a frequency range of 0.2–0.02 Hz in 10 splits.

AE

The single lap-joint shear tests were performed on an Instron Universal Testing Machine equipped with a 30-kN load shell. The extension rate was 1.3 mm min^{-1} . In Fig. 5, the experimental setup for the mechanical test with the concurrent AE monitoring is depicted. The AE activity was recorded on-line during the test using two wide band AE sensors (R-15-ALPHA, Physical Acoustics Corp., PAC) that were attached on the same side of the specimen, as shown in Fig. 5. A layer of medical ultrasonic gel was applied between the sensors and the specimen to provide acoustic coupling. Due to the specific sensors sensitivity to frequencies from 100 up to 600 kHz, they can capture a wide range of different sources. The pre-amplifier gain was set to 40 dB. After performing a pilot test, the threshold was also set to 40 dB in order to



4 Experimental setup for the IRT, a IR camera, b IR lamps, c specimen, d IR excitation voltage



5 Experimental setup for the lap-shear test. Instron testing machine a, specimen b, AE sensors c

avoid the possibility of electronic/environmental noise. The signals were recorded in a two-channel monitoring board PCI-2, PAC with a sampling rate of 5 MHz.

Healing process

After it was monitored with IRT, the purposefully damaged film was healed by placing in an oven at 150°C, i.e. the required temperature for the specific system for the retro-DA reaction to take place. Afterwards it was left to cool down to room temperature and was monitored again using IRT. In the case of the lap joint, after the shear failure of the joint, the specimens were ‘healed’ by reassembling the broken joint and placing between heating plates for 5 min. The healing temperature of the plates was again constant at 150°C. The healed lap-joint specimens were left to cool down for 3 h and they were retested under the same loading conditions. At this point the second reaction that is required for the self-healing process of DA was completed.

Results and discussion

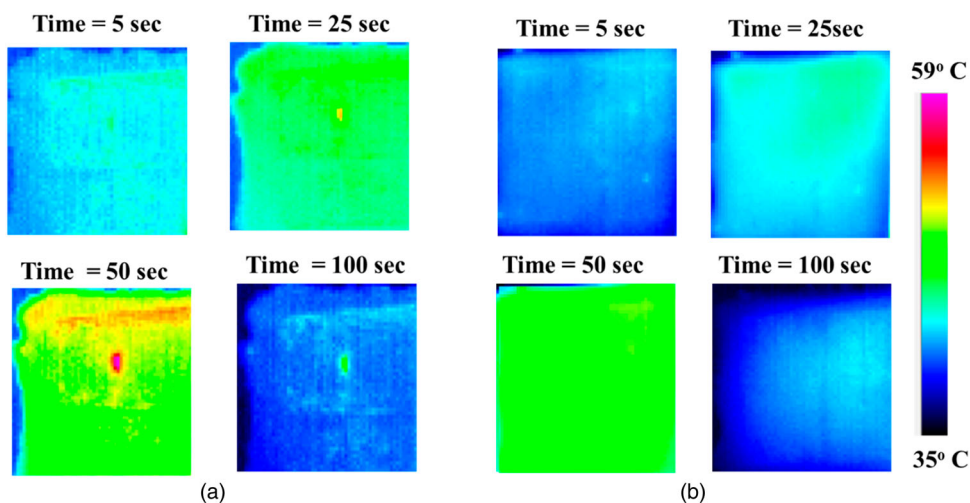
IRT

The BMI-1700 with the TF employed as a cross-linker was employed for the IRT monitoring. As aforementioned, the experimental process involved the purposeful

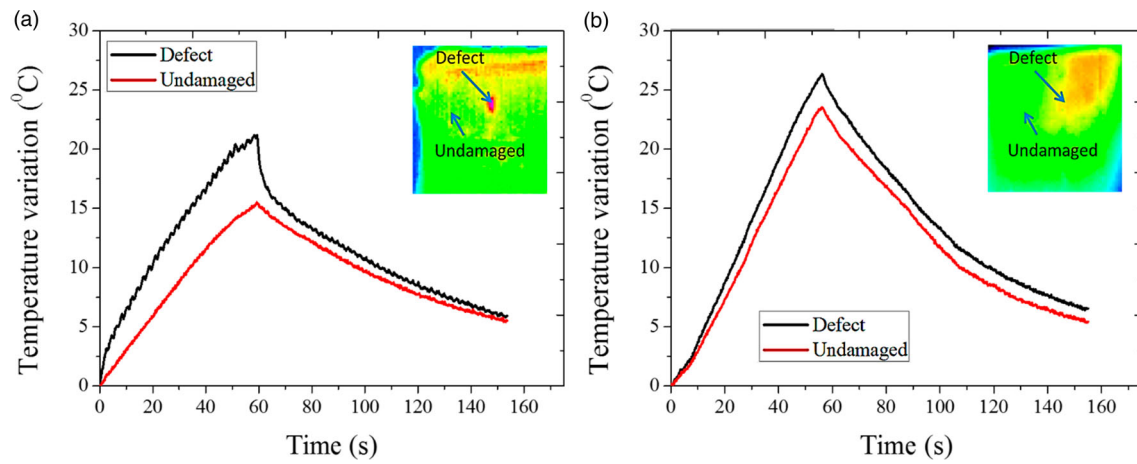
creation of an artificial defect on the surface of the film. The defect was introduced as described in Section ‘Materials’ in order to monitor the response of the defect area after one healing event. Figure 6 presents the real-time temperature profile at specific time intervals of the real-time thermographic recording for the damaged (Fig. 6a) and healed (Fig. 6b) film.

In Fig. 6a, the specimen before healing can be observed and the artificial defect is clearly revealed. The imprint of the defect in the thermograph is depicted as a heat trap in the dynamic heating process, i.e. it is not visible at the beginning of the IR excitation and is barely visible immediately afterwards, but can be clearly seen after the thermal excitation is maximum at approximately the end of the IR heating cycle (i.e. 50 s) and is fading afterwards as the heat is dissipating and the temperature gradients are disappearing with time. On the other hand in Fig. 6b the defect ceases to exist after the healing event resulting in a uniformly distributed thermal behaviour. It is worth noting that although the heating of the surface of the specimen is relatively uniform, there are distinct areas (see Fig. 6a, time = 50 s) that may also be regarded as potential damaged sites, although no such indication was seen during the manufacturing and the creation of the artificial defect.

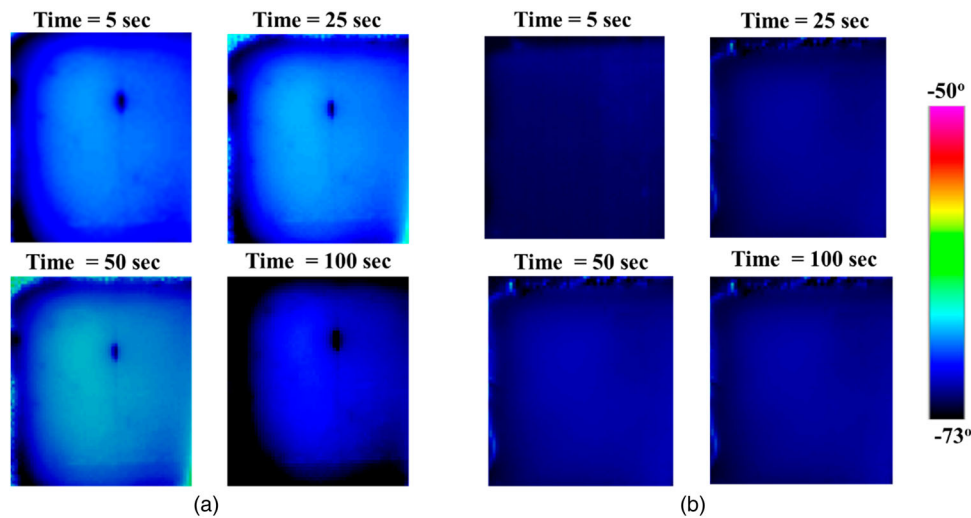
In Fig. 7 the timegraphs depict more clearly that the damaged area before the healing cycle has a totally



6 Thermographs obtained using pulsed thermography for the virgin a and healed b specimen



7 Timegraphs of temperature variations of the a virgin and b healed specimen



8 Phase images from the damaged a and healed b specimen

different thermal behaviour than the undamaged area. Timegraphs depict an average temperature in a selected format from the camera pixel area which in this case was selected to be a two-by-two pixel area in the defect site and away from it.

The differences are depicted not only by the different thermal intake rates but also from the accumulated thermal energy that the damaged area has absorbed. On the other hand after the healing process, the thermal behaviour of the entire material is the same and the defect cannot be detected. It should be pointed out that the thermal signature of the specimen after the healing cycle (damaged and undamaged area) is still presenting a relative difference, both in maximum temperature and cumulative absorption of thermal energy although no distinct differences can be discerned in the distinct thermographs.

Figure 8 presents the phase images for the respective times of the heating cycle. Whereas temperature and amplitude graphs relate to the local temperature gradients, phase images relate to the phase difference of the thermal waves emitted from the specimen surface. Indicative of the different approach is that (i) the phase images reveal the existence of the flaw even at the beginning of the heating cycle with a clear phase difference fluctuating around approximately 5° (Fig. 8a) and (ii) there is clearly no indication of the previous existence of the flaw after healing of the specimen.

The timegraphs in Fig. 9 confirm the above observations, clearly pinpointing the existence of the flaw from the initial phase images (Fig. 9a) and proving that as there is no trace of the artificially created flaw, the specimen has fully healed (Fig. 9b).

Recapitulating, the studied material was successfully healed when in film form. Pulsed phase thermography was successful in ascertaining that there are practically no differences between the virgin and the healed area after one healing cycle. The phase images practically eliminated all artefacts mostly provoked by the inhomogeneity of IR excitation, to reveal a fully healed surface.

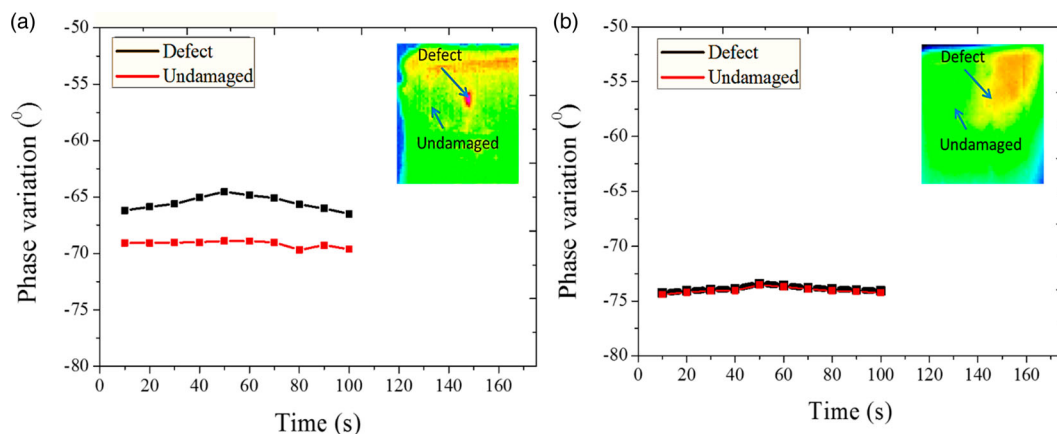
Shear strength – healing efficiency

As described in ASTM, *D 1002*, the apparent shear strength of the lap joints was calculated using equation (1).

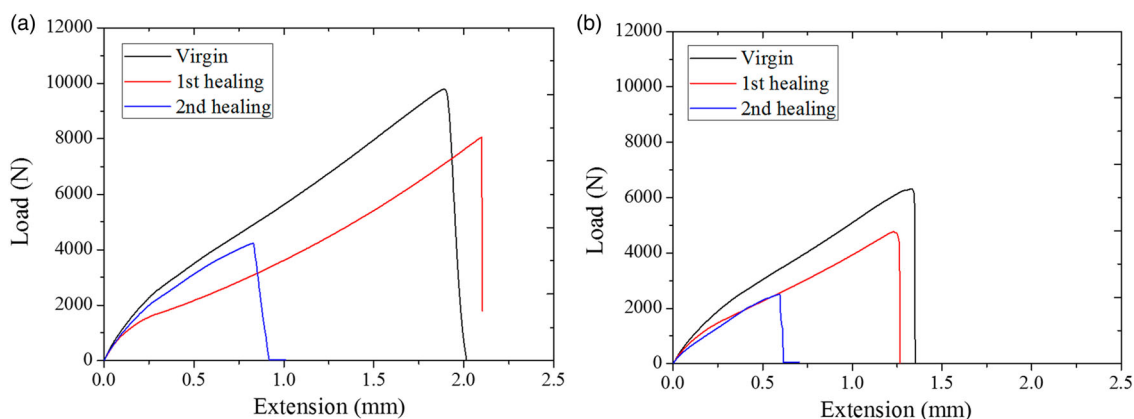
$$\tau_{\max} = \frac{L_{\max}}{A} \tag{1}$$

where τ_{\max} is the shear strength expressed in MPa, L_{\max} is the maximum load in N and A is the bond area in square millimetre.

In Fig. 10a and b, load vs. extension curves for the virgin and healed BMI-1700 and BMI-1500 (first and second healing cycle) are depicted, respectively. The healing



9 Timegraphs of phase variations of the a virgin and b healed specimen



10 Load vs. extension curves after two healing cycles. a BMI-1700, b BMI-1500

efficiency was calculated by deriving the maximum shear strength of the healed material τ_h and the maximum shear strength of the virgin material τ_v as obtained from the tensile tests (equation (2)).

$$n = \frac{\tau_h}{\tau_v} \tag{2}$$

In detail, a total healing efficiency of 82.2% for the BMI-1700 specimen and 75.5% for BMI-1500 specimen corresponding to the first healing cycle. Both BM-1700 and BMI-1500 exhibit high values of healing efficiency for the first healing cycle and a notable value of healing efficiency for the second healing cycle was calculated. Healing efficiencies of BMI-1700 and BMI-1500 are summarised in detail in Table 1.

As can be seen in Fig. 10a and b, the load vs. displacement curves of all specimens exhibit typical brittle behaviour as expected. Changes in the slope of the curves are present for the healed specimens which are more obvious for the BMI-1700 case and the first healing cycle did not affect significantly the materials when we study the maximum extension. On the other hand, the second healing affected more the materials resulting in much less maximum extension. In addition, based on the aforementioned figures, BMI-1700 appears to have superior adhesive behaviour when compared to BMI-1500 (Table 1).

The examination of the fracture area of all specimens (virgin and healed) exhibited mixed mode failure meaning

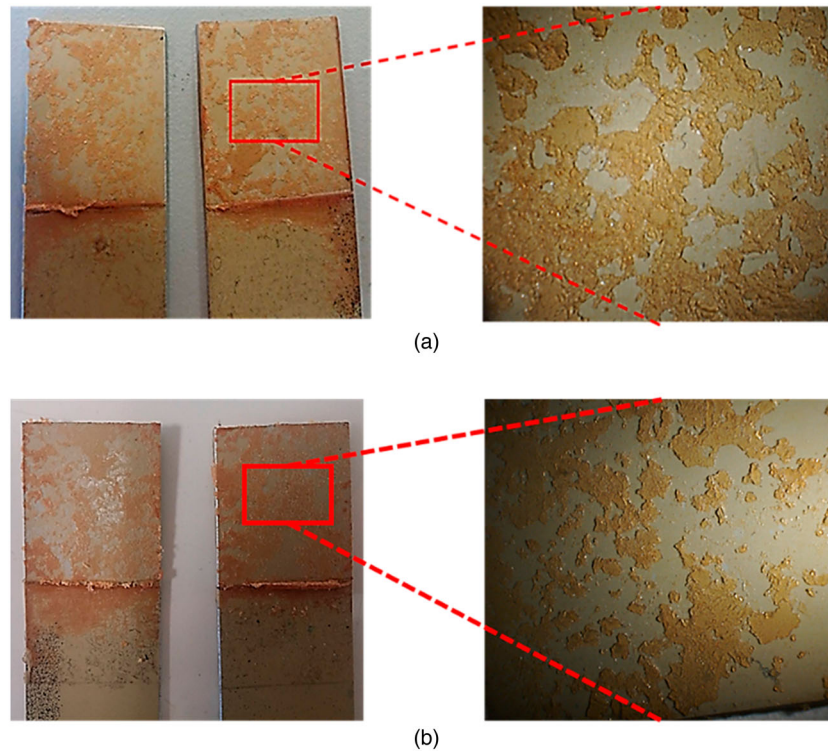
that both adhesive and cohesive failure were present (Fig. 11). Some areas of the joint failed in an adhesive manner at the primer coating/adhesive interface while other areas failed in a cohesive manner through the mass of the adhesive material. As can be seen in Fig. 11, no significant differences in the type of failure between the two polymeric systems are present.

AE

Figure 12 summarises the AE profile of the virgin and healed BMI-1700 for three sequential lap-joint shear tests, i.e. virgin, healed once and healed twice. The chosen descriptors to describe the fracture process are (i) cumulative hits which are indicative of the overall activity, (ii)

Table 1 Maximum load, maximum shear strength and healing efficiencies of BMI-1700

	Sequence	L_{max}/N	τ/MPa	Healing efficiency/%
BMI-1700	Virgin	9791.9	13.43	
	First healing	8054.9	11.04	82.2
	Second healing	4233.6	5.80	43.2
BMI-1500	Virgin	6320.91	8.66	
	First healing	4770.197	6.54	75.5
	second healing	2512.83	3.44	39.7



11 Stereographs obtained from the single lap-joint fractured surfaces of a BMI-1700 and b BMI-1500

absolute energy of the recorded waveforms which are indicative of the energy content of the transient stress wave and (iii) RA value which is the ration of rise time to amplitude for each recorded waveform. The RA value is indicative of the type of fracture that occurs in the monitored volume.²⁷ In general, lower RA values respond to mode I fractures and higher RA values to mode II fracture. This phenomenological observation has been confirmed for a variety of material systems and is based on the assumption that for the same crack length, mode I cracks release more energy in unit time and therefore their acoustic signature is characterised by higher amplitude and lower rise time.^{27–29} For comparison purposes, a moving average is included in all index population together with the recorded load curve as the second y axis.

As can be seen in the case of the virgin polymeric system all AE signal indices indicate a typical brittle failure. For almost the entire duration of the mechanical testing, AE activity, absolute energy and RA values exhibit a plateau on the respective graphs followed by an abrupt increase just before the final fracture of the adhesive.

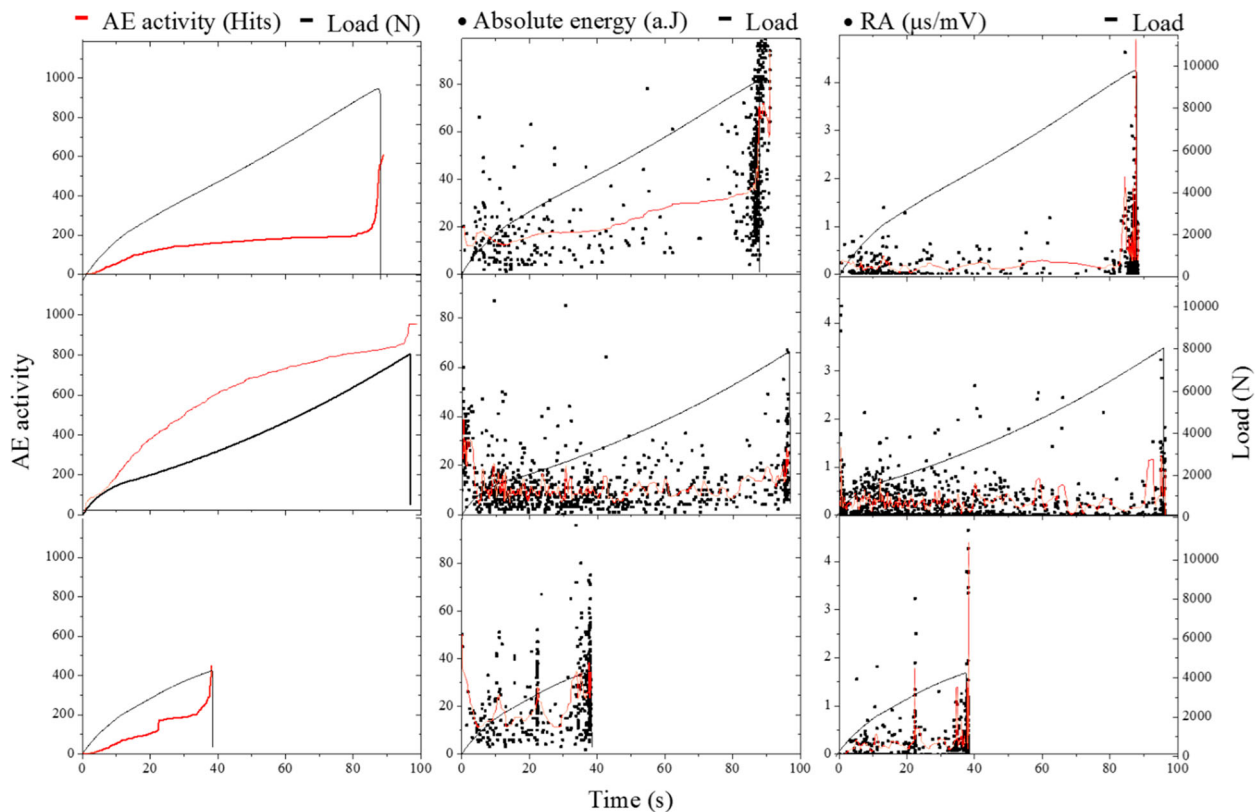
On the other hand, the acoustic profile of the material after the first healing cycle exhibits a different behaviour. The cumulative hit number rises to reach asymptotically a value of approximately 800 and further on exhibits a step increase which is marginally sustained until failure. This denotes a two-stage failure which may be attributed to a transition from a typical brittle failure to a more compliant one after the first healing cycle. It can be postulated that the appearance of this stepwise activity may be due to a more stable propagation of the interlaminar crack from the edges of the joint, which allows for a less brittle failure and the recording of a second AE activity stage. Further, the moving average curve of the absolute energy loses the tendency to increase that exhibited during the

testing of the virgin material. Similarly the RA value is fluting at higher averages suggesting an overall less brittle failure than in the case of the virgin specimen.

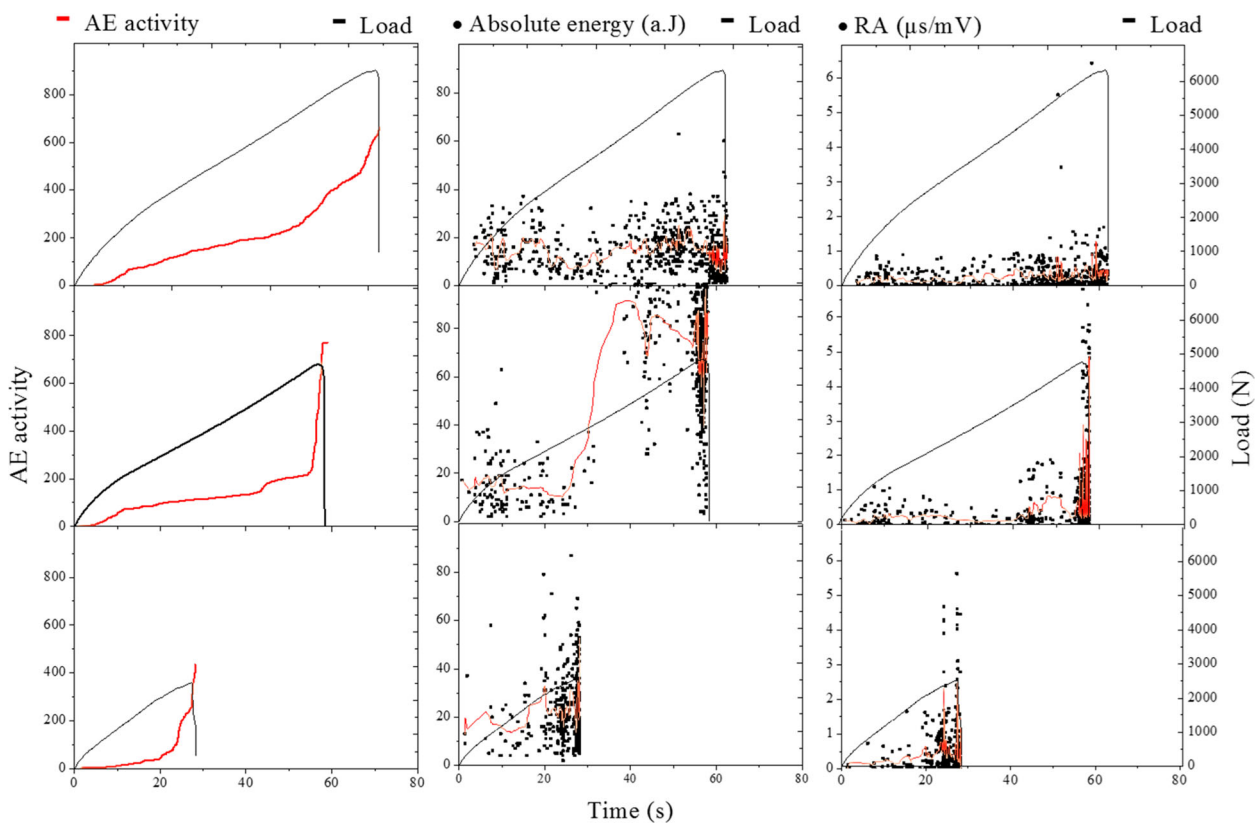
After the second healing event the quasi-toughening effect is even more distinctly manifested in the two-phase failure attributed to stable mode-II crack propagation from the edges of the adhesive. This failure can also be observed on the moving average lines of the absolute energy and RA at approximately 20 and 40 s of testing where two distinctive spikes are present. The differentiations in the AE profile can be attributed to changes in the material's internal state and more specifically to possible degradation of the polymer due to thermal treatment during the healing process, which alters the three-dimensional cross-linking network of the epoxy and contributes to the aforementioned quasi-toughening behaviour.

For the case of BMI-1500, obtained results indicate that the AE profile of the self-healing system exhibits a different behaviour than that of BMI-1700 (both virgin and healed) in terms of cumulative AE hits absolute energy and RA values (Fig. 13). In detail, for the virgin BMI-1500, the cumulative AE hits curve exhibits a two-stage curve indicating in its turn a two-phase failure. Again it may be assumed that the two phases correspond to an initial stage where failure is manifested in the form of microcracking within the polymer and a second phase where a crack is propagating stably from the edges of the lap joint. In contrast to the BMI-1700, the BMI-1500 exhibits this behaviour already in its virgin state and this may be attributed to the lower molecular weight of BMI-1500 compared to that of BMI-1700. For the virgin material, the absolute energy and RA value do not exhibit significant variations until the failure of the specimen.

After the first healing cycle, the two-stage failure is still observed, but the acoustic activity becomes considerable just prior to failure. In this respect, we may assume that



12 Acoustic activity vs. time for the BMI-1700 adhesive joint: rows represent in sequence a virgin, b first healing cycle and c second healing cycle. Columns represent in sequence a hits, b absolute energy and c RA value



13 Acoustic activity vs. time for the BMI-1500 adhesive joint: rows represent in sequence a virgin, b first healing cycle and c second healing cycle. Columns represent in sequence a hits, b absolute energy and c RA value

healing has the opposite effect to that of BMI-1700, i.e. it tends to suppress the two-phase behaviour. Moreover, the absolute energy values indicate an abrupt fourfold increase which precedes the appearance of the second phase in the acoustic activity. Finally, the RA value exhibits a considerable increase prior to failure, something that was not noted in the failure of the virgin specimen. The acoustic activity of the lap joint after the second healing exhibits similar behaviour to that of the lap joint after the first healing, albeit scaled down to lower values due to the earlier failure of the joint. Again a two-stage behaviour is noticed, together with an increase in absolute energy and RA value at the second stage, albeit less prominent in this case.

Overall, the BMI-1500 exhibits a more consistent acoustic activity after the healing cycles compared to that of BMI-1700, indicating that there are smaller changes associated with the failure 'signature' of the lap joint. Overall, the AE study indicates a failure mode shift in the case of BMI-1700 which is attributed to the change in the 3D cross-linking network of the high molecular weight polymer. It should be however again noted that the BMI-1700 performs significantly better compared to the BMI-1500, and this suggested change in its failure mode is less detrimental to its healing efficiency with successive healing cycles, as is clearly shown in Table 1.

Conclusions

The present work involved the study of two self-healing polymeric systems (BMI-1700 and BMI-1500) used as adhesives in a metal-to-metal single lap-joint tension testing. AE was also employed in order to quantitatively identify the virgin vs. 'healed' specimen under the same loading conditions through the comparison of the acoustic signal before and after healing.

IRT was successfully utilised in order to evaluate and assess the healing performance of the polymeric material. As it was shown a defect was successfully repaired resulting in a uniform thermal behaviour. Local temperature variations due to the defect were recorded in the case of the virgin BMI-1700 but not in the case of the healed one indicating a complete recovery of the initial state of the material. As was pointed out, phase images are successful in diminishing the effect of non-uniform excitation which may create artefacts irrelevant to the material state.

Both self-healing polymers exhibited high values of healing efficiencies for the first healing cycle and notable healing efficiencies for the second healing cycle. The BMI-1700 in particular exhibited particularly high self-healing efficiencies retaining almost 50% of its initial lap-shear strength even after two healing cycles. In addition, all specimens (virgin and healed) exhibited mixed mode failure meaning that both adhesive and cohesive failure was present.

AE corresponded to the identification of the acoustic signature of damage and its correlation to healing. The healing process, being essentially a quasi-reversible process, had a noticeable effect to indices like absolute energy and RA value of the AE signal, providing a measure of differentiation in failure mode between the virgin and the healed specimen, particularly in the case of BMI-1700, where differences in the acoustic signature

suggested a change in failure mode, attributed to the change of the three-dimensional polymer network after successive healing cycles.

Acknowledgements

The authors acknowledge the 'THALES-GSRT ID I.D:593 Mis: 379412' research program for financial support. The self-healing polymers were synthesised in the Theoretical & Physical Chemistry Institute, National Hellenic Research Foundation, within the framework of the 'THALES-GSRT ID I.D: 593 Mis: 379412' research program.

ORCID

A. S. Paipetis  <http://orcid.org/0000-0001-9668-9719>

References

1. D. G. Bekas, K. Tsirka, D. Baltzis and A. S. Paipetis: 'Self-healing materials: a review of advances in materials, evaluation, characterization and monitoring techniques', *Compos. Part B*, 2016, **87**, 92–119.
2. G. Postiglione, S. Turri and M. Levi: 'Effect of the plasticizer on the self-healing properties of a polymer coating based on the thermoreversible Diels–Alder reaction', *Prog. Org. Coat.*, 2015, **78**, 526–531.
3. J. S. Park, T. Darlington, A. F. Starr, K. Takahashi, J. Riendeau and H. Thomas Hahn: 'Multiple healing effect of thermally activated self-healing composites based on Diels–Alder reaction', *Compos. Sci. Technol.*, 2010, **70**, (15), 2154–2159.
4. J. Kötteritzsch, S. Stumpf, S. Hoepfner, J. Vitz, M. D. Hager and U. S. Schubert: 'One-component intrinsic self-healing coatings based on reversible crosslinking by Diels–Alder cycloadditions', *Macromol. Chem. Phys.*, 2013, **214**, (14), 1636–1649.
5. W. Zhang, J. Duchet and J. F. Gerard: 'Self-healable interfaces based on thermo-reversible Diels–Alder reactions in carbon fiber reinforced composites', *J. Colloid Interf. Sci.*, 2014, **430**, 61–68.
6. J. Ax and G. Wenz: 'Thermoreversible networks by Diels–Alder reaction of cellulose furoates with bismaleimides', *Macromol. Chem. Phys.*, 2012, **213**, (2), 182–186.
7. J. Brancart, G. Scheltjens, T. Muselle, B. Van Mele, H. Terryn and G. Van Assche: 'Atomic force microscopy-based study of self-healing coatings based on reversible polymer network systems', *J. Intel. Mat. Syst. Str.*, 2012, **25**, (1), 40–46.
8. B. J. Adzima, C. J. Kloxin and C. N. Bowman: 'Externally triggered healing of a thermoreversible covalent network via self-limited hysteresis heating', *Adv. Mater.*, 2010, **22**, (25), 2784–2787.
9. X. Chen, M. A. Dam, K. Ono, A. Mal, H. Shen, S. R. Nutt, K. Sheran and F. Wudl: 'A thermally re-mendable cross-linked polymeric material', *Science*, 2002, **295**, (5560), 1698–1702.
10. X. Chen, F. Wudl and A. Mal: 'New thermally remendable highly cross-linked polymeric materials', *Macromolecules*, 2003, **38**, 1802–1808.
11. C. Toncelli, D. C. De Reus, F. Picchioni and A. A. Broekhuis: 'Properties of reversible Diels–Alder furan/maleimide polymer networks as function of crosslink density', *Macromol. Chem. Phys.*, 2012, **213**, (2), 157–165.
12. G. Rivero, L.-T. T. Nguyen, X. K. D. Hillewaere and F. E. Du Prez: 'One-pot thermo-remendable shape memory polyurethanes', *Macromolecules*, 2014, **47**, (6), 2010–2018.
13. S. Khoee and Z. Kachoei: 'Design and development of novel reactive amine nanocontainers for a self-healing epoxy adhesive: self-repairing investigation using the lap shear test', *RSC Adv.*, 2015, **5**, (27), 21023–21032.
14. D. T. Everitt, R. Luterbacher, T. S. Coope, R. S. Trask, D. F. Wass and I. P. Bond: 'Optimisation of epoxy blends for use in extrinsic self-healing fibre-reinforced composites', *Polymer*, 2015, **69**, 283–292.
15. G. C. Huang, J. K. Lee and M. R. Kessler: 'Evaluation of norbornene-based adhesives to amine-cured epoxy for self-healing applications', *Macromol. Mater. Eng.*, 2011, **296**, (10), 965–972.

16. J. H. Aubert: 'Note: Thermally removable epoxy adhesives incorporating thermally reversible diels-alder adducts', *J. Adhesion*, **2003**, **79**, (6), 609–616.
17. A. Carpinteri, F. Cardone and G. Lacidogna: 'Energy emissions from failure phenomena: mechanical, electromagnetic, nuclear', *Exp. Mech.*, **2010**, **50**, 1235–1244.
18. D. T. G. Katerelos, A. Paipetis, T. Loutas, G. Sotiriadis, V. Kostopoulos and S. L. Ogin: 'In situ damage monitoring of cross-ply laminates using acoustic emission', *Plast. Rubber Compos.*, **2009**, **38**, (6), 229–234.
19. S. A. Grammatikos, E. Z. Kordatos, T. E. Matikas and A. S. Paipetis: 'Real-time debonding monitoring of composite repaired materials via electrical, acoustic, and thermographic methods', *J. Mater. Eng. Perform.*, **2013**, **23**, (1), 169–180.
20. X. P. Maldague: 'Introduction to NDT by active infrared thermography', *Mater. Eval.*, **2002**, **60**, (9), 1060–1073.
21. E. Z. Kordatos, D. A. Exarchos, K. G. Dassios and T. E. Matikas: 'Thermo-electrical lockin thermography for characterization of sub-surface defects', *Proc. SPIE*, **2014**, **9062**, 90620G.
22. S. A. Grammatikos, E. Z. Kordatos, N. M. Barkoula, T. E. Matikas and A. S. Paipetis: 'Innovative non-destructive evaluation and damage characterisation of composite aerostructures using thermography', *Plast. Rubber Compos.*, **2011**, **40**, (6–7), 342–348.
23. R. A. Chowdhury, M. V. Hosur, M. Nuruddin, A. Tcherbi-Narteh, A. Kumar, V. Boddu and S. Jeelani: 'Self-healing epoxy composites: preparation, characterization and healing performance', *J. Mater. Res. Technol.*, **2015**, **4**, (1), 33–43.
24. Y.-L. Liu and C.-Y. Hsieh: 'Crosslinked epoxy materials exhibiting thermal remendability and removability from multifunctional mal-imide and furan compounds', *J. Polym. Sci. Pol. Chem.*, **2006**, **44**, 905–914.
25. I. ASTM: 'D 1002 – Standard test method for apparent shear strength of single-lap-joint adhesively bonded metal specimens by tension loading (metal-to-metal); **2001**.
26. I. ASTM: 'D 3933 – Standard guide for preparation of aluminum surfaces for structural adhesives bonding; **1998**.
27. D. G. Aggelis, N. M. Barkoula, T. E. Matikas and A. S. Paipetis: 'Acoustic structural health monitoring of composite materials: damage identification and evaluation in cross ply laminates using acoustic emission and ultrasonic', *Compos. Sci. Technol.*, **2012**, **72**, (10), 1127–1133.
28. N. K. Paschos, D. G. Aggelis, N. M. Barkoula, A. S. Paipetis, T. E. Matikas and A. D. Georgoulis: 'Rupture of anterior cruciate ligament monitored by acoustic emission', *J. Acoust. Soc. Am.*, **2011**, **129**, (6), 217–222.
29. D. G. Aggelis, D. V. Soulioti, N. Sapouridis, N. M. Barkoula, A. S. Paipetis and T. E. Matikas: 'Acoustic emission characterization of the fracture process in fibre reinforced concrete', *Constr. Build. Mater.*, **2011**, **25**, (11), 4126–4131.